**Article:**
Skipper, W. orcid.org/0000-0001-8315-2656, Meierhofer, A., Chalisey, A. et al. (2 more authors) (2024) Generation of sanded creep curves using the extended creep force model with high pressure torsion data. Wear, 542-543. 205278. ISSN 0043-1648

https://doi.org/10.1016/j.wear.2024.205278

Wear 542-543 (2024) 205278

Contents lists available at ScienceDirect

Wear

journal homepage: www.elsevier.com/locate/wear

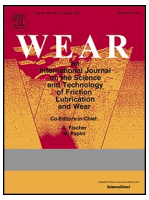

# Generation of sanded creep curves using the extended creep force model with high pressure torsion data

W. Skipper [a,*], A. Meierhofer [b], A. Chalisey [c], K. Six [b], R. Lewis [a]

[a] Leonardo Centre for Tribology, The University of Sheffield, Sheffield, S1 3JD, UK
[b] Virtual Vehicle Research GmbH, Inffeldgasse 21a, 8010, Graz, Austria
[c] RSSB, The Helicon, One South Place, London, UK

ARTICLE INFO

*Keywords:*
Wheel/rail interface
Creep curves
Tribological testing
Sanding
Low adhesion
Modelling

ABSTRACT

In this paper an approach for generating predicted full-scale creep force – creep curves from small-scale tribological tests has been outlined and examples produced using rail sands and low adhesion contaminants. A high pressure torsion rig was used to measure the change in shear stress over increasing displacement for British and Austrian rail sands in dry, wet, and leaf contaminated conditions under different normal pressures. In addition, tests with just sycamore leaf powder and graphite were also conducted. This data was then used to parameterise extended creep force models for each contact condition, from which predictions of full-scale behaviour were then made and validated using full-scale data from literature.

## 1. Introduction

Traction in the wheel/rail contact (traction is referred to as "adhesion" in the rail industry) controls the amount of braking and acceleration available to a train. In low adhesion conditions, the available traction is low and this can result in timetable delays [1] and safety issues [2], which contribute to the cost of low adhesion to the British rail industry to be estimated at ~£355 m/annum [3]. The application of sand is one common method for mitigating against low adhesion conditions [4].

Predicting real-world traction behaviour from small-scale tests is a cost effective way of assessing different low adhesion contaminants (e.g. leaves) and mitigations thereof. In addition, there are indirect benefits to sustainability arising from this approach. A more cost-effective method for predicting the effect on traction of new adhesion materials would allow for alternatives to sand (an unsustainable material) to be more easily assessed.

Small-scale simulations of the wheel/rail contact have historically been focussed on twin-disc testing [5–12]. The advantages of twin-disc testing over field testing are the lower associated costs and better control of variables (weather conditions, third body application, etc.). However, the smaller contact area of the twin-disc set-up compared to actual wheel/rail contacts and the constant recycling of the same material over many cycles led to questions over the relevance of the data generated when using it to predict full-scale behaviour. Testing the impact of granular third body materials (e.g. sand) on the contact is a particular problem with small discs being used. It has been found that the impact can be overstated due to: the discs artificially recycling the continuously applied granular material creating a layer of sand and/or mixing with wear debris to form a third body layer [5,12]; and the different contact geometry between discs, such as the different nip geometry between the discs and the smaller contact area [11], when compared to the wheel and rail. In addition, it is harder to control the amount of material getting into the contact.

A different test method for assessing friction in the wheel/rail interface, that solves some of the problems associated with twin-disc testing, whilst maintaining the greater economy compared to field testing, is the high pressure torsion (HPT) method. HPT rigs have traditionally been used to test the effects of high strain rates on materials [13–16], but have recently been used to also study the wheel/rail contact [17,18]. In addition, recent work has been done to study the effects of rail sand [18–20], and top of rail products [21] on tribological performance.

HPT data can be used to parameterise, for example, the extended creep force (ECF) model, which can then generate accurate predictions of full-scale behaviour [22,23]. The aim of this paper was to extend the ECF model to predict behaviour of two different rail sands (British & Austrian), as well as two low adhesion contaminants (sycamore leaf and

* Corresponding author.
*E-mail address:* W.Skipper@sheffield.ac.uk (W. Skipper).

https://doi.org/10.1016/j.wear.2024.205278
Received 22 February 2023; Received in revised form 22 January 2024; Accepted 26 January 2024
Available online 28 January 2024

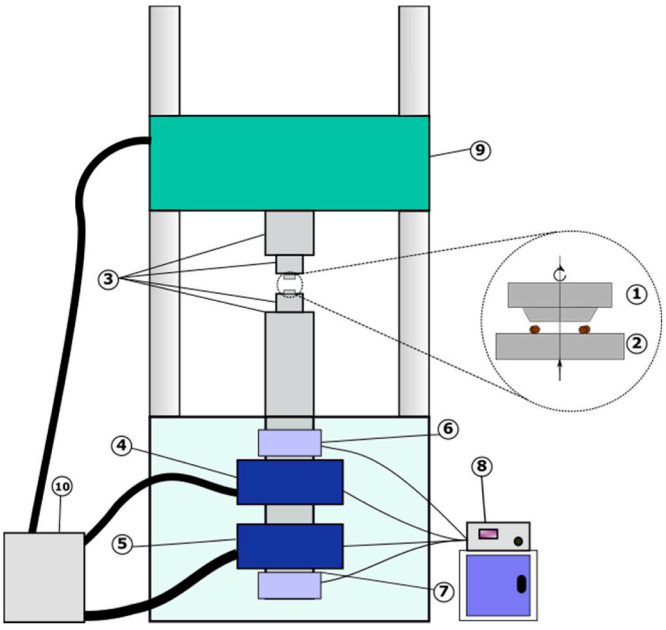


**Fig. 1.** Full schematic of the high pressure torsion rig [19].

**Fig. 2.** Example of particle application [18].

graphite, the latter representing coal dust [24]).

## 2. Methodology

### 2.1. High pressure torsion

A schematic of the HPT method is included in Fig. 1. The wheel and rail specimens (1 & 2 respectively) were fixed into specimen holders (3). Initially, the specimens were out of contact, but were brought together during testing and a normal pressure was applied using the axial hydraulic actuator (4) (with the axial displacement and force output measured by a linear variable differential transducer/load cell (6)), creating an annular contact. Once requisite normal pressure was achieved, the specimen faces were then rotated against each other using a rotational hydraulic actuator (5), with the rotational displacement and torque output measured by a rotational variable differential transducer/load cell (7). These movements are regulated by the attached controller (8), and pressurised via a hydraulic ring main (10); movement of the crosshead (9) allows for room to apply third body layers. The third body layer being applied into the contact between the wheel and rail

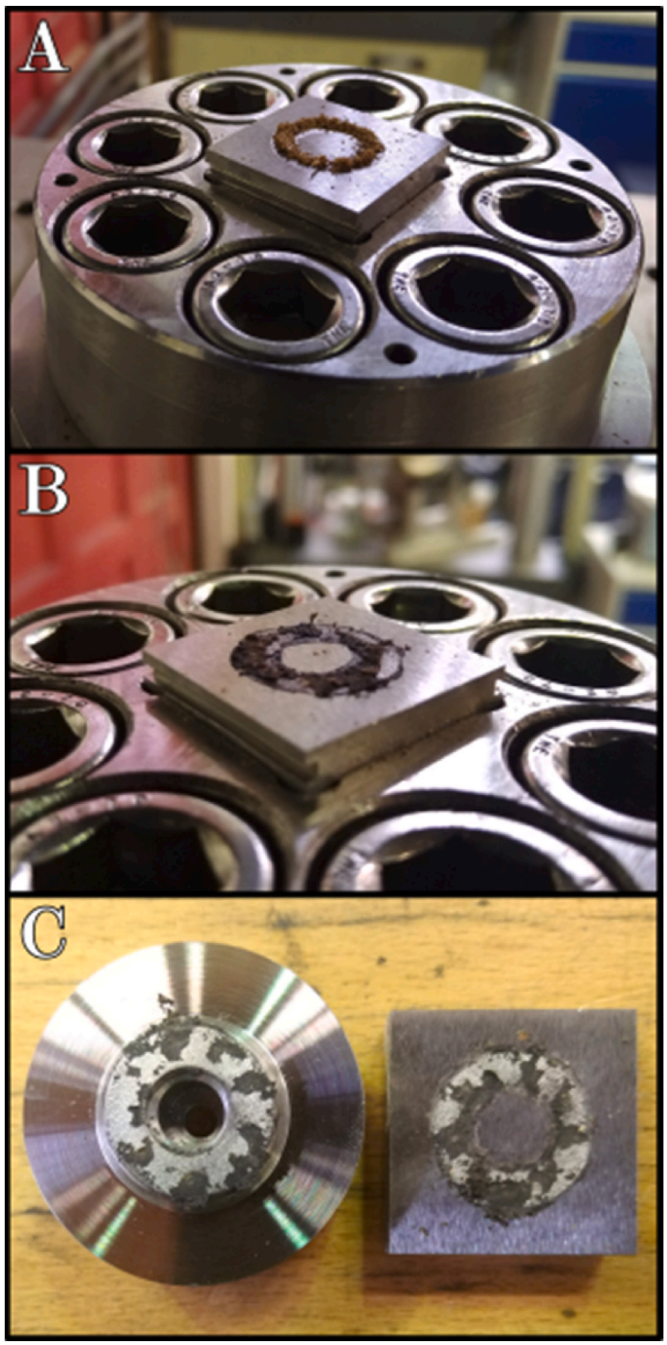


**Fig. 3.** Formation of leaf layer in the HPT rig: (A) Initial application of dry leaf powder, (B) after initial run-in, (C) Post test runs.

**Table 1**
Summary of particle characteristics for GB & at rail sands.

| Characteristic | GB | AT |
|---|---|---|
| $D_{50}$ (mm) | 1.56 | 1.03 |
| Circularity | 0.87 | 0.79 |
| Hardness (GPa) | 12.2 ± 2.0 | 8.1 ± 2.1 |

specimen changed the amount of torque needed to turn through a set sweep angle. A full description of the HPT method can be found in previous work by Evans et al. [17].

Third body materials applied to the HPT in this work were added after the surfaces of the top and bottom specimen were run-in and

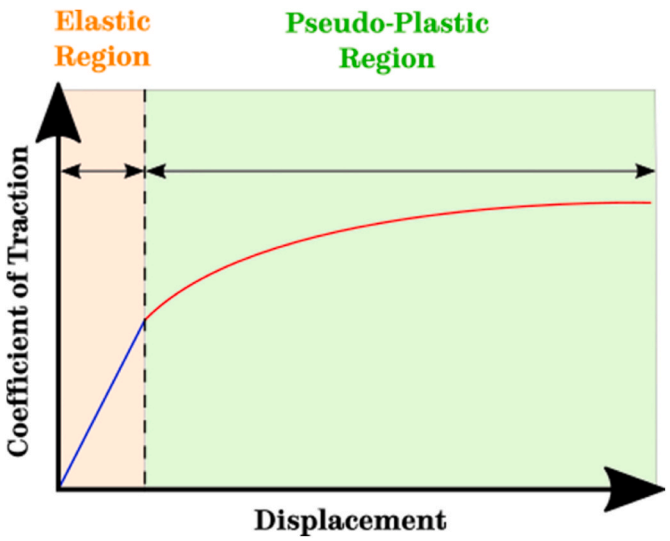


**Fig. 4.** Typical example of HPT output [19].

traction peaked at a constant level, this run-in procedure was previously defined by Evans et al. [17]. The sand particles were applied in quantities of 0.025 g (consistent with the maximum amount of sand permitted on the rail head, 7.5 g/m, according to GMRT 2461 [25]), an example of this application can be seen in Fig. 2.

For tests in wet conditions, 20 μl of distilled water was applied by pipette ensuring an even spread around the contact; any rail sand was applied at the same time. For both sycamore leaf and graphite powder tests, 0.025 g of material was applied with 20 μl of distilled water; one sweep was undertaken to run-in the low adhesion layer after which any rail sand was applied as well as another 20 μl of distilled water. The formation of the layer is included in Fig. 3.

HPT tests were performed using British rail sand (GB) and Austrian rail sand (AT) (sourced from respective local depots). Particle characteristics, including shape, size, and hardness can be found in previous work [19,26], and a summary has been added in Table 1. Each rail sand was tested under three different normal pressures (300, 600, & 900 MPa) and in dry, wet, and leaf contaminated conditions.

In addition, tests were performed with Sycamore leaf powder and graphite under the same aforementioned normal pressures. The sycamore leaf powder was collected from fallen leaves in Sheffield and blended and filtered through a 160 μm sieve (full details of this process can be found in Ref. [27]). Graphite powder was sourced from "Alfa Aesar" with an average particle size of 7–11 μm at 99 % purity. (CAS no.: 7782-42-5).

Repeat tests were conducted for all combinations of test conditions.

The typical output of a single HPT test run has been included in Fig. 4, where displacement refers to rotational displacement through the effective radius of friction (see Ref. [17] for detail) and coefficient of traction refers to the ratio between shear load and normal load. The “elastic” region (ER) is characterised by an initial steep linear increase. The “pseudo-plastic” region (PPR) begins when asperity level contacts begin to plastically deform, work hardening the contact and leading to the coefficient of traction continuing to increase in the PPR. This asperity level plasticity was referred to as “local” or “tribological” plasticity by Six et al. [28], who also specify that this plasticity should not be confused with “global” plasticity, i.e. plastic deformation in the bulk material. For clarification: “global” plasticity can occur in the HPT contact during initial load cycles until reaching a shakedown limit. When a "real" 3rd body layer exists (e.g. leaf, sand) in the contact, this PPR may also be a function of asperity deformation and plasticity within the real 3rd body layer, though the interplay between these factors is an area of ongoing research.

**Table 2**
Average peak coefficient of traction at varying normal pressures in dry conditions with british and austrian rail sands.

| Normal Pressure (MPa) | Average Peak CoT | |
|---|---|---|
| | GB | AT |
| 300 | 0.61 | 0.52 |
| 600 | 0.66 | 0.54 |
| 900 | 0.75 | 0.59 |

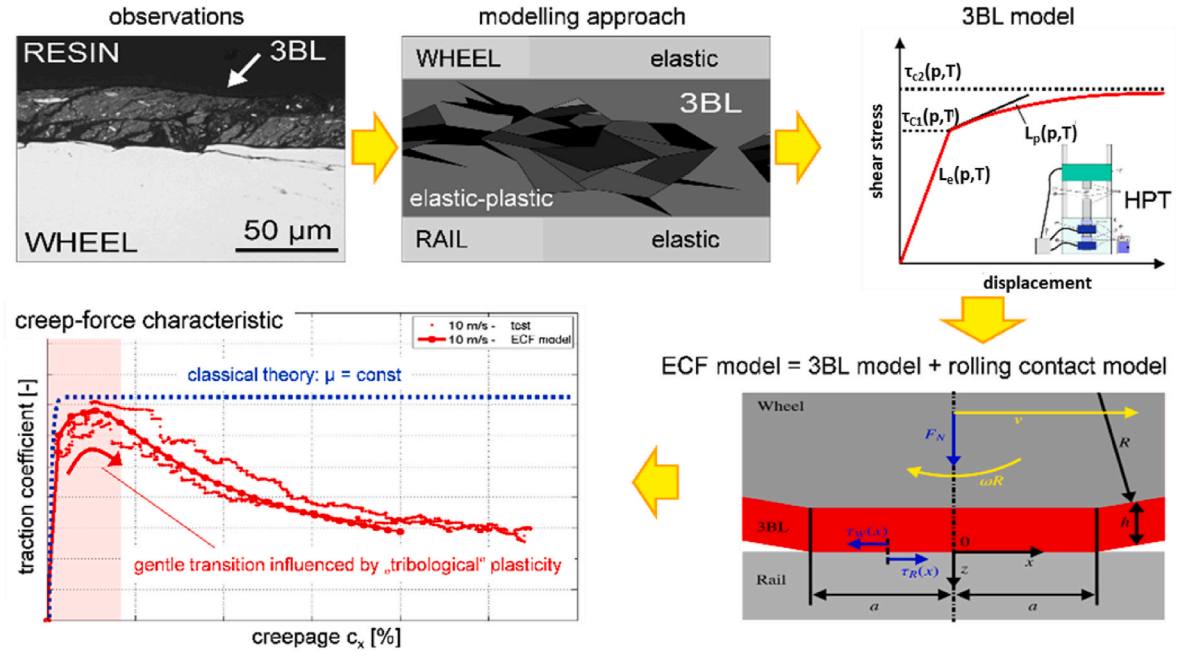


**Fig. 5.** Ecf model: Approach and Methodology [17].

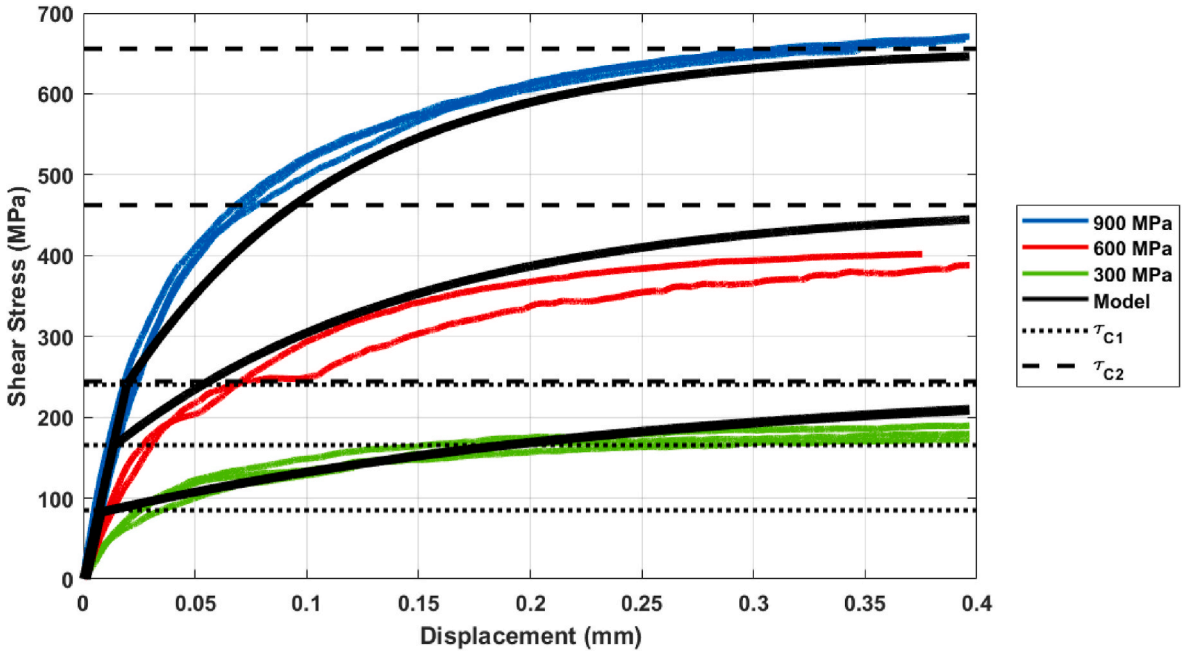


**Fig. 6.** Ecf fit for dry tests with British rail sand.

**Table 3**
ECF input parameters for dry conditions with british rail sand.

| Material Parameter | Nominal | Pressure Dependency |
|---|---|---|
| $L_e$ | 0.252 µm/GPa | $\infty$ $GPa^{-1}$ |
| $L_p$ | 0.0381 mm | 0.548 $GPa^{-1}$ |
| $\tau_{C1}$ | 1.49 GPa | 0.195 $GPa^{-1}$ |
| $\tau_{C2}$ | 2.16 GPa | 0.401 $GPa^{-1}$ |

### 2.2. Extended creep force model

#### 2.2.1. Model description

Fig. 5 summarises the modelling approach of the ECF model. This model is used to predict the creep force characteristic of wheel-rail contacts (see bottom left subplot). It is based on the idea that there is always a third body layer (3BL) between wheel and rail, which has been confirmed by lab and field experiments (see e.g. top left subplot). The

**Table 4**
ECF input parameters for dry conditions with austrian rail sand.

| Material Parameter | Nominal | Pressure Dependency |
|---|---|---|
| $L_e$ | 0.252 µm/GPa | $\infty$ $GPa^{-1}$ |
| $L_p$ | 0.136 mm | 1.64 $GPa^{-1}$ |
| $\tau_{C1}$ | 0.228 GPa | 0.972 $GPa^{-1}$ |
| $\tau_{C2}$ | 1.37 GPa | 0.583 $GPa^{-1}$ |

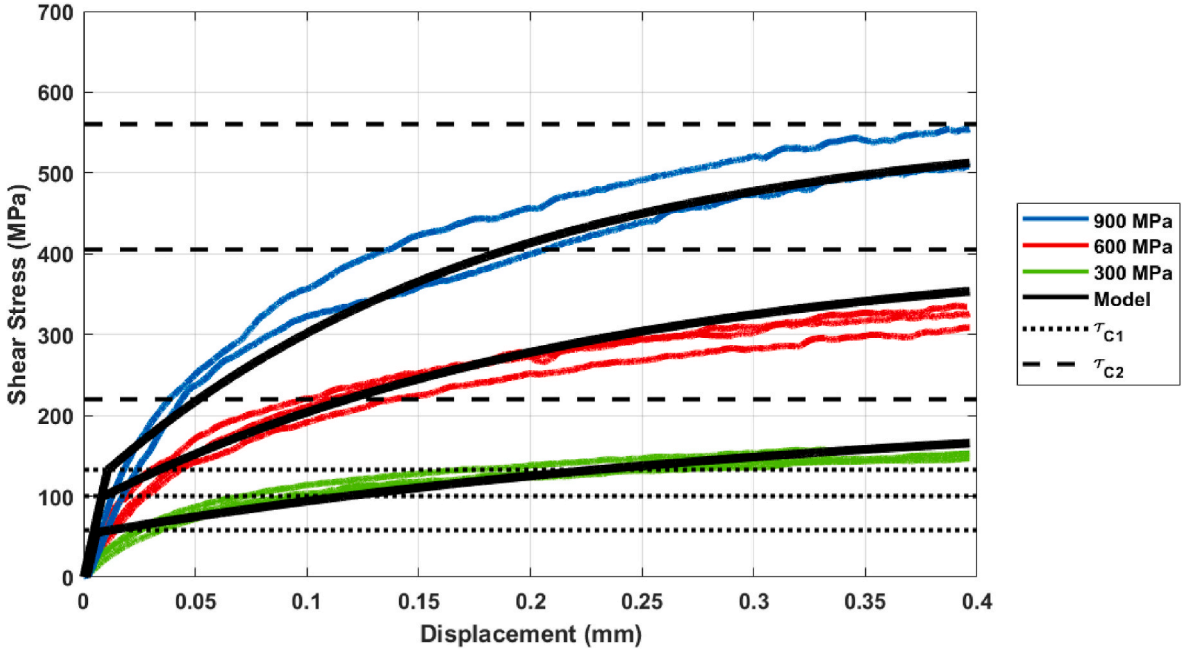


**Fig. 7.** Ecf fit for dry tests with austrian rail sand.

**Table 5**
Average peak coefficient of traction at varying normal pressures in wet conditions with british and austrian rail sands.

| Normal Pressure (MPa) | Average Peak CoT | |
|---|---|---|
| | GB | AT |
| 300 | 0.48 | 0.45 |
| 600 | 0.54 | 0.50 |
| 900 | 0.61 | 0.51 |

3BL in the model comprises "real" 3BLs (sand particles, wear debris, iron oxides, etc.) and the near-surface layers of wheel and rail including roughness and the related "tribological" plasticity phenomena [28]. It is assumed that the wheel and the rail behave elastically, while the 3BL is assumed to have an elastic-plastic behaviour (see top centre subplot). This 3BL is described using a brush model, which consists of independent "bristles" perpendicular to the contact plane, with tangential stiffness considered to be constant along each bristle [29].

The ECF model can thus be described, in the simplest of terms, using two equations. Equation (1) defining shear stress in the elastic region, and Equation (2) defining shear stress in the pseudo-plastic region using Voce's hardening law [30]:

$$\underline{\tau} = \frac{\underline{u_3}}{L_e} \; for \; \underline{\tau} \leq \tau_{C1} \qquad \text{Equation 1}$$

$$|\underline{\tau}| = \tau_{C1} + (\tau_{C2} - \tau_{C1})\left[1 - exp\left(\frac{-|\underline{u_3}| + \tau_{C1}L_e}{L_p}\right)\right] \; for \; \tau_{C1} < |\underline{\tau}| < \tau_{C2} \qquad \text{Equation 2}$$

where $\underline{\tau} = (\tau_x, \tau_y)$ and represents shear stress acting upon a bristle, $\underline{u_3}$ represents the displacement of a bristle. The parameters $\tau_{C1}$, $\tau_{C2}$, $L_e$, & $L_p$ are described below and are shown graphically in Fig. 5 (top right subplot).

- The critical shear stresses at which the contact begins to act pseudo-plastically and at which the maximum shear stress is recorded ($\tau_{C1}$, $\tau_{C2}$ respectively);
- The inverted elastic stiffness i.e. initial slope of the graph ($L_e$);
- The plasticity factor i.e. the shape of the curve in the pseudo-plastic region ($L_p$).

These four parameters are considered to be dependent on contact pressure and temperature dependency (top right subplot).

This 3BL brush model (bottom right subplot) can be used to predict the creep force characteristic (bottom left subplot). The ECF model is able to describe measured characteristics much better than classical theory e.g. falling friction at high creepage, a gentle transition from a steep linear region to a saturated region, speed and load dependency, etc. A detailed description of the model can be found in Refs. [12,22,28].

### 2.2.2. Parameterisation

When parameterising the ECF model using HPT data there are 12 constants that can be identified using empirical methods. These constants include the critical thresholds ($\tau_{C1}$ and $\tau_{C2}$), inverted elastic stiffness ($L_e$) and a plasticity factor ($L_p$), where each of these four parameters can be characterised by the three functions of nominal, pressure dependent and temperature dependent values (notated with a superscript 0, p, and T respectively), thus equating to 12 parameters in total.

High pressure torsion (HPT) data can parameterise nominal and pressure dependent values, via conducting tests at three different normal pressures and fitting the corresponding Voce-Material law [22]. Nominal values are physical measurements of the layer, where $\tau_{c1}^0, \tau_{c2}^0, L_e^0, L_p^0$ represent the maximum yield stress, maximum shear strength, minimum inverted stiffness, and minimum plasticity factor of the 3rd body layer respectively.

With respect to the critical shear stresses, as the HPT can be thought of as a one-dimensional experiment with rotation as the only degree of

**Table 6**
ECF input parameters for wet conditions with british rail sand.

| Material Parameter | Nominal | Pressure Dependency |
|---|---|---|
| $L_e$ | 0.252 μm/GPa | $\infty\ GPa^{-1}$ |
| $L_p$ | 0.0217 mm | 0.326 $GPa^{-1}$ |
| $\tau_{C1}$ | 0.826 GPa | 0.219 $GPa^{-1}$ |
| $\tau_{C2}$ | 3.90 GPa | 0.166 $GPa^{-1}$ |

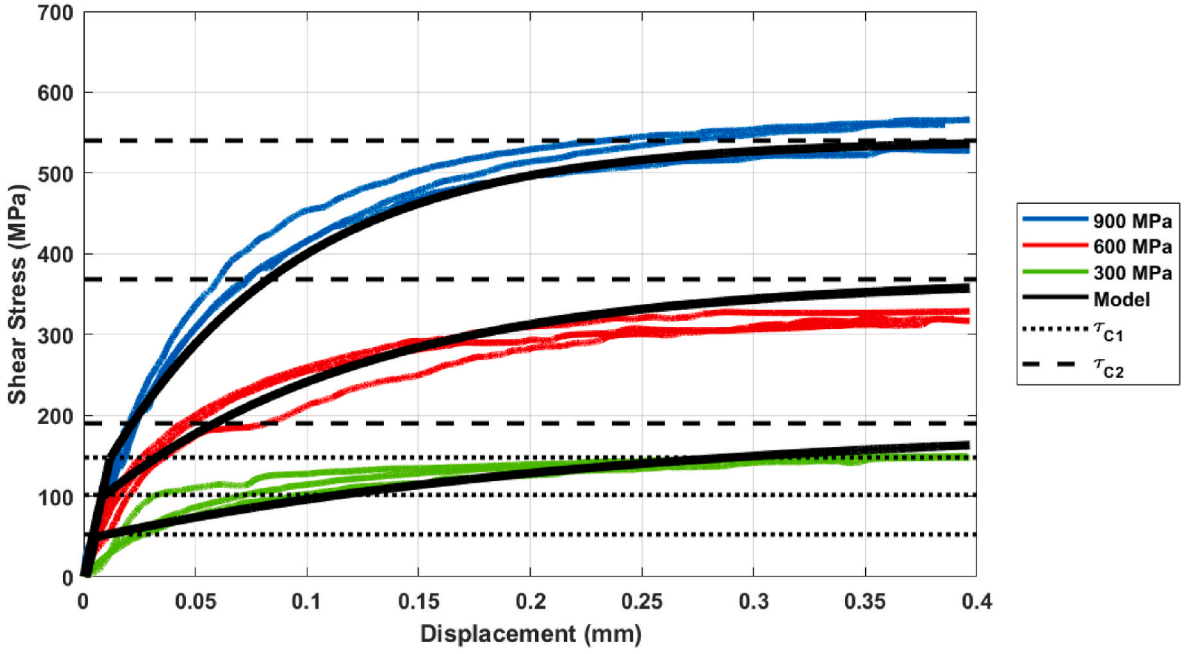


**Fig. 8.** Ecf fit for wet tests with British rail sand.

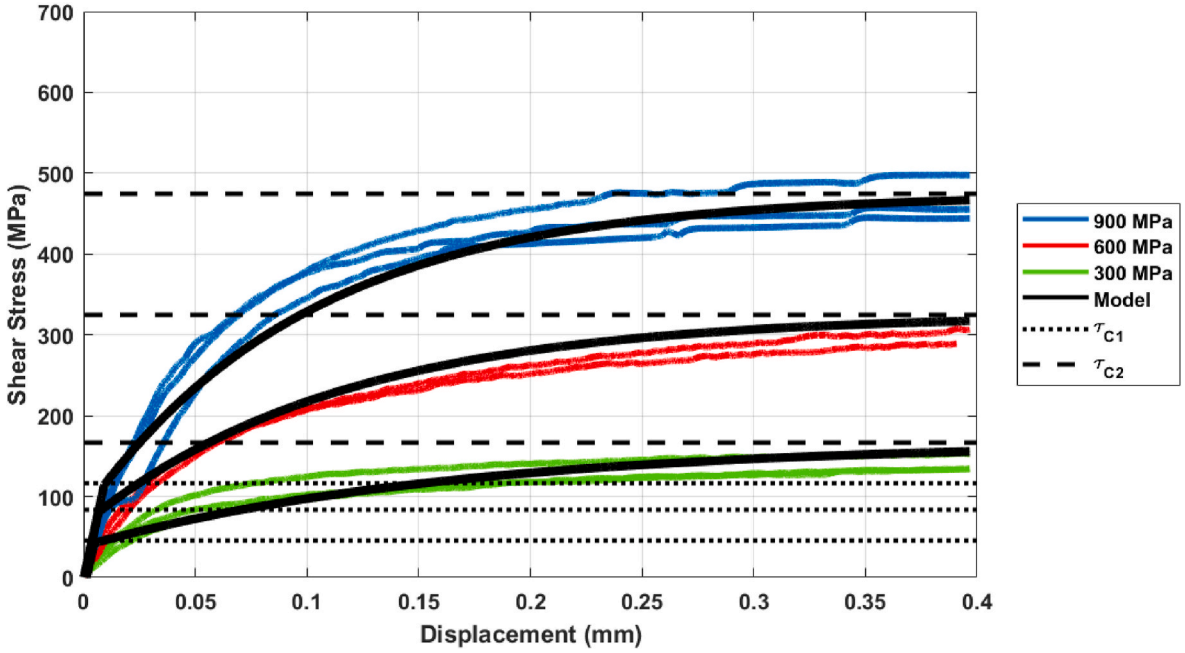


**Fig. 9.** Ecf fit for wet tests with austrian rail sand.

**Table 7**
ECF input parameters for wet conditions with austrian rail sand.

| Material Parameter | Nominal | Pressure Dependency |
|---|---|---|
| $L_e$ | 0.252 μm/GPa | $\infty\ GPa^{-1}$ |
| $L_p$ | 0.0911 mm | 2.70 $GPa^{-1}$ |
| $\tau_{C1}$ | 0.276 GPa | 0.609 $GPa^{-1}$ |
| $\tau_{C2}$ | 2.90 GPa | 0.199 $GPa^{-1}$ |

**Table 8**
Average peak coefficient of traction at varying normal pressures in leaf contaminated conditions with british and austrian rail sands.

| Normal Pressure (MPa) | Average Peak CoT | |
|---|---|---|
| | GB | AT |
| 300 | 0.22 | 0.19 |
| 600 | 0.20 | 0.16 |
| 900 | 0.13 | 0.14 |

movement, it is considered that the shear force in the contact is equivalent to that of a linear test. Especially as the displacement during a test (0.4 mm) is much smaller than its effective radius of friction (~7.5 mm) and thus curvature can be neglected.

The temperature dependency of the parameters was supplied by Meierhofer [22], and was acquired from vehicle tests running in the high creepage regime to observe falling friction effects. These temperature dependent parameters are fed into a temperature sub-model thereby allowing for the prediction of full-scale behaviour [17] (more details of which are in Ref. [22]). As the HPT operates at very low sweep rates, and thus low contact temperatures [23], it is not possible to directly parameterise temperature dependency using this method.

A more detailed overview of the HPT/ECF approach can be found in Ref. [22], where the detail behind linking physical characteristics to the 12 parameters is included.

British and Austrian rail sands (GB and AT respectively) were used to parameterise the ECF model for dry, wet, and leaf contaminated conditions. Each contact condition was tested on the HPT test rig at three different normal pressures (300, 600, & 900 MPa) to fully characterise the pressure dependency; repeat tests were conducted for each test condition. In addition, this same process was repeated to parameterise the ECF model with low adhesion contaminants (sycamore leaf and graphite). All ECF model predictions were made assuming a train with a 110 kN wheel load running at 5 m/s.

## 3. Results

### 3.1. High pressure torsion data & parameterisation

The following section details the ECF parameterisation process undertaken with HPT data. For each contact condition, a figure showing HPT traction data and the fit of the model has been included. In addition, the calculated parameters are also presented for each condition.

#### 3.1.1. Dry sanded conditions

From HPT tests it is possible to measure the Coefficient of Traction (CoT), i.e. the ratio between shear stress and normal pressure. Table 2 reports the peak CoTs for British and Austrian rail sands under varying normal pressures. It can be noted that peak CoTs for AT rail sand were lower than for GB rail sand, possibly due to the material being less hard (12.2 ± 2.0 GPa for GB & 8.1 ± 2.1 GPa for AT [19]). In addition, there appears to be a pressure dependency for both rail sands, with higher normal pressures creating higher CoTs.

Using dry sanded data, rig stiffness (flexion in the rig between the HPT surface and the load cell measuring torque) was optimised and calculated to be 80 $\mu$m/GPa. This value was used throughout the parameterisation processes for all contact conditions.

The ECF model for data from tests with GB rail sand in dry conditions has been included in Fig. 6, where the relative error of the model fit was calculated as 8.4 %. This error was calculated using the coefficient of variation of the root mean square error (RMSE), such that:

$$\epsilon = 100 \bullet \frac{\sqrt{mean\left(\left[\kappa - \widehat{\kappa}\right]^2\right)}}{mean(\kappa)} \qquad \text{Equation 3}$$

where $\widehat{\kappa}$ represents model predictions and $\kappa$ the experimental values.

$L_e^0$ was not optimised and remained as the value calculated by Meierhofer [22]. In addition, pressure dependency on $L_e$ was neglected by Meierhofer [22], thus $L_e = \infty$ $GPa^{-1}$ was also used throughout this study. The model appears to fit very well at higher contact pressures,

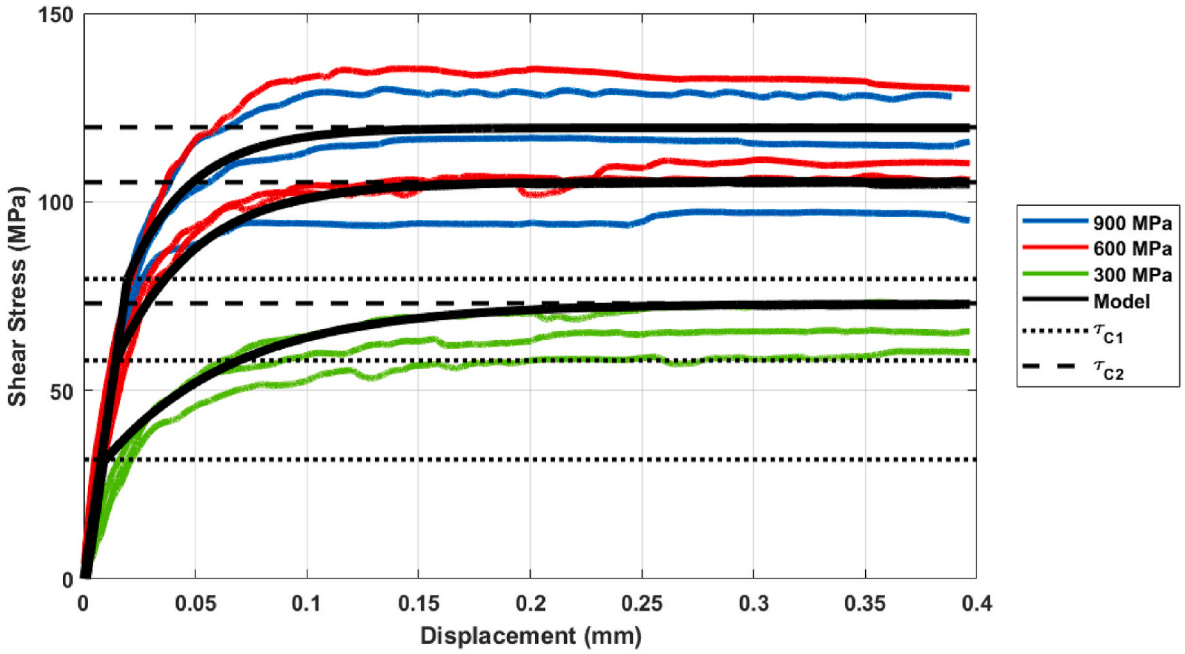


**Fig. 10.** Ecf fit for leaf contaminated tests with British rail sand.

**Table 9**
ECF input parameters for leaf contaminated conditions with british rail sand.

| Material Parameter | Nominal | Pressure Dependency |
|---|---|---|
| $L_e$ | 166 μm/GPa | $\infty\ GPa^{-1}$ |
| $L_p$ | 0.0208 mm | 1.45 $GPa^{-1}$ |
| $\tau_{C1}$ | 0.182 GPa | 0.636 $GPa^{-1}$ |
| $\tau_{C2}$ | 0.131 GPa | 2.72 $GPa^{-1}$ |

with stiffness becoming increasingly over-estimated at lower contact pressures. The critical stresses appear to fit very well to the HPT data at all normal pressures.

The parameterisation of dry data with GB rail sand produced the input parameters included in Table 3. These parameters are of a similar order of magnitude to previous parameterisation processes that were performed by Meierhofer [22] and Evans [23].

Fig. 7 shows the ECF model parameterised by HPT data produced in

**Table 10**
ECF input parameters for leaf contaminated conditions with austrian rail sand.

| Material Parameter | Nominal | Pressure Dependency |
|---|---|---|
| $L_e$ | 80.0 μm/GPa | $\infty\ GPa^{-1}$ |
| $L_p$ | 0.0170 mm | 93.1 $GPa^{-1}$ |
| $\tau_{C1}$ | 0.0201 GPa | 2.07 $GPa^{-1}$ |
| $\tau_{C2}$ | 0.180 GPa | 1.27 $GPa^{-1}$ |

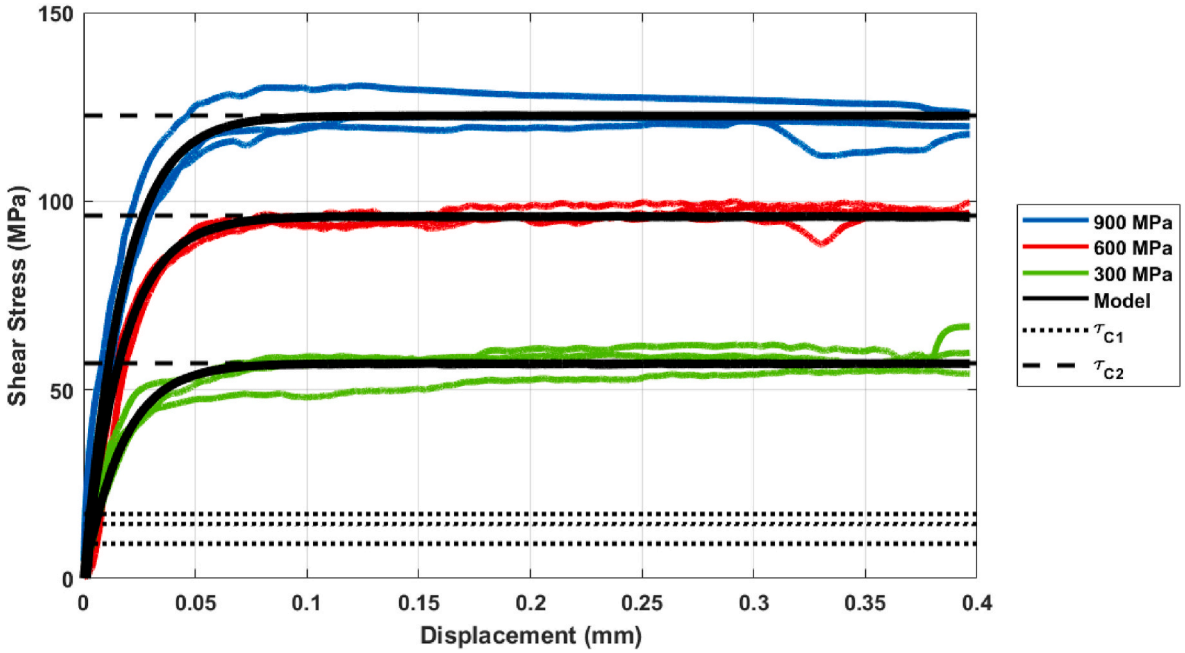


**Fig. 11.** Ecf fit for leaf contaminated tests with austrian rail sand.

**Table 11**
Average peak coefficient of traction at varying normal pressures in low adhesion conditions.

| Normal Pressure (MPa) | Average Peak CoT | |
|---|---|---|
| | Sycamore | Graphite |
| 300 | 0.06 | 0.04 |
| 600 | 0.05 | 0.03 |
| 900 | 0.05 | 0.03 |

dry conditions with Austrian rail sand. The relative error of the model was 9.7 %, with the accuracy of the initial stiffness of the model again becoming lower with decreasing normal pressure. The parameters from the dry model with AT rail sand are shown in Table 4.

### 3.1.2. Wet sanded conditions

The peak CoTs in wet conditions are presented in Table 5, where the values are generally lower than observed for dry conditions (see Table 2). Similar to dry conditions, GB produced higher peak CoTs than AT and both rail sands saw increasing normal pressures produce higher CoTs.

The ECF model for wet, GB sanded HPT data has been included in Fig. 8, where a relative error value of 7.6 % was obtained. $L_e^0$ was not optimised, as was the case for the previous dry models. The fit is very similar to that seen in dry, sanded conditions, with an increasingly over-estimated stiffness at lower contact pressures, but with a good fit to critical shear stresses. The input parameters from wet, sanded conditions are included in Table 6. They remain a similar order of magnitude as the input parameters calculated from dry, sanded HPT data.

The ECF model generated from wet, AT sanded data is included in Fig. 9; a relative error of 9.0 % was calculated. The slight overestimation in stiffness, which increased with decreasing normal pressure is still apparent. Input parameters from the wet, AT sanded model have been included in Table 7.

### 3.1.3. Leaf contaminated sanded conditions

The peak CoTs in leaf contaminated conditions with sand applied are presented in Table 8, where CoTs are much lower when compared to dry and wet conditions (see Table 2 & Table 5). The difference in CoT between GB and AT was much less pronounced in leaf contaminated conditions, with GB even being lower than AT at 900 MPa. Previous work found that adhesion mitigation in a leaf contaminated contact was most dependent on particle size instead of hardness [19]; as the rail sands were of different sizes this may explain the differences seen here. In comparison to dry and wet conditions where increasing normal pressure resulted in higher CoTs, the opposite is true in the leaf contaminated contact, possibly due to the interaction between sand particles and a physical leaf layer.

As opposed to dry and wet, sanded conditions, $L_e^0$ was optimised for leaf contaminated conditions, due to the large differences in stiffnesses in these conditions. The ECF model fitting is included in Fig. 10, where a relative error value of 14.5 % was calculated. As can be seen when comparing to previous dry, and wet models, the introduction of sycamore leaf powder has drastically decreased the measured shear stresses. Overall, the fitting is relatively accurate, though there is still some slight over-estimation of stiffness at lower contact pressures. The calculated input parameters have been included in Table 9. $L_e^0$ has risen by a few degrees of magnitude compared to the stiffness calculated for dry and wet conditions. Other input parameters maintain similar orders of magnitude.

The ECF model produced from leaf contaminated, AT sanded HPT data is included in Fig. 11, where the relative error was 4.5 %. The calculated shear stresses are similar to those seen for leaf contaminated, GB sanded HPT tests, though there appears to be greater consistency in the data between changes in normal pressure. The parameters obtained from the fitting process for leaf contaminated, AT sanded conditions are included in Table 10.

**Table 12**
ECF Input Parameters for Leaf Contaminated Conditions with No Adhesion Material applied.

| Material Parameter | Nominal | Pressure Dependency |
|---|---|---|
| $L_e$ | 57.1 μm/GPa | $\infty$ $GPa^{-1}$ |
| $L_p$ | 0.0156 mm | 1.09 $GPa^{-1}$ |
| $\tau_{C1}$ | 0.0147 GPa | 3.14 $GPa^{-1}$ |
| $\tau_{C2}$ | 0.420 GPa | 0.120 $GPa^{-1}$ |

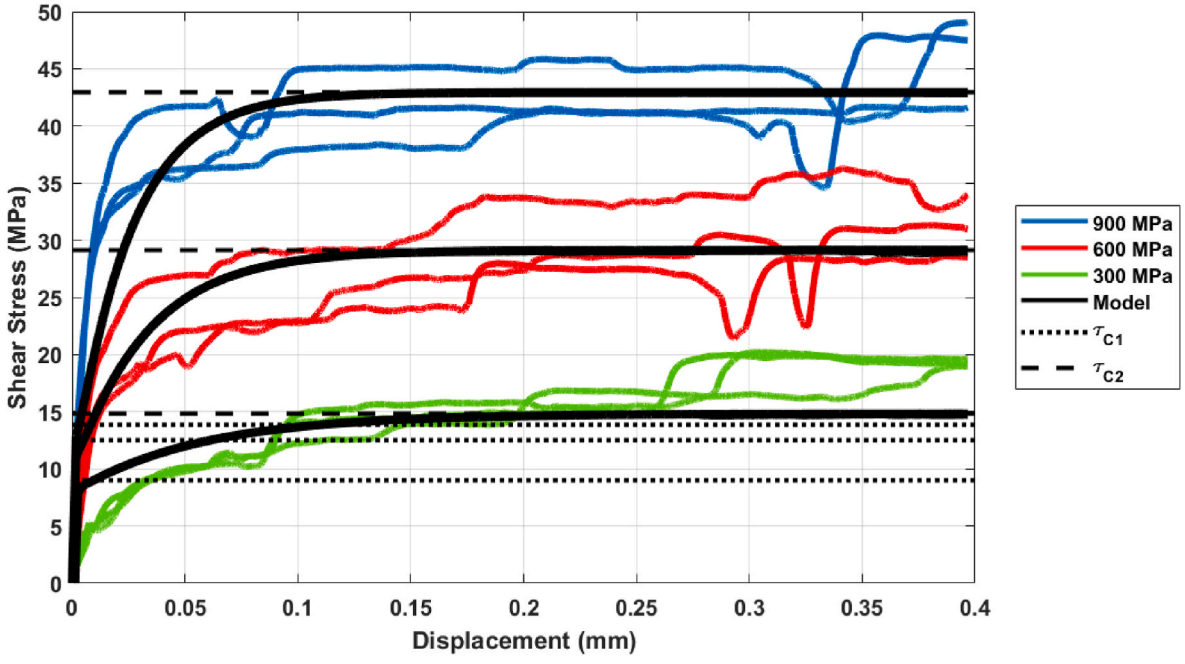


**Fig. 12.** ECF Fit for Leaf Contaminated Tests with No Adhesion Material applied.

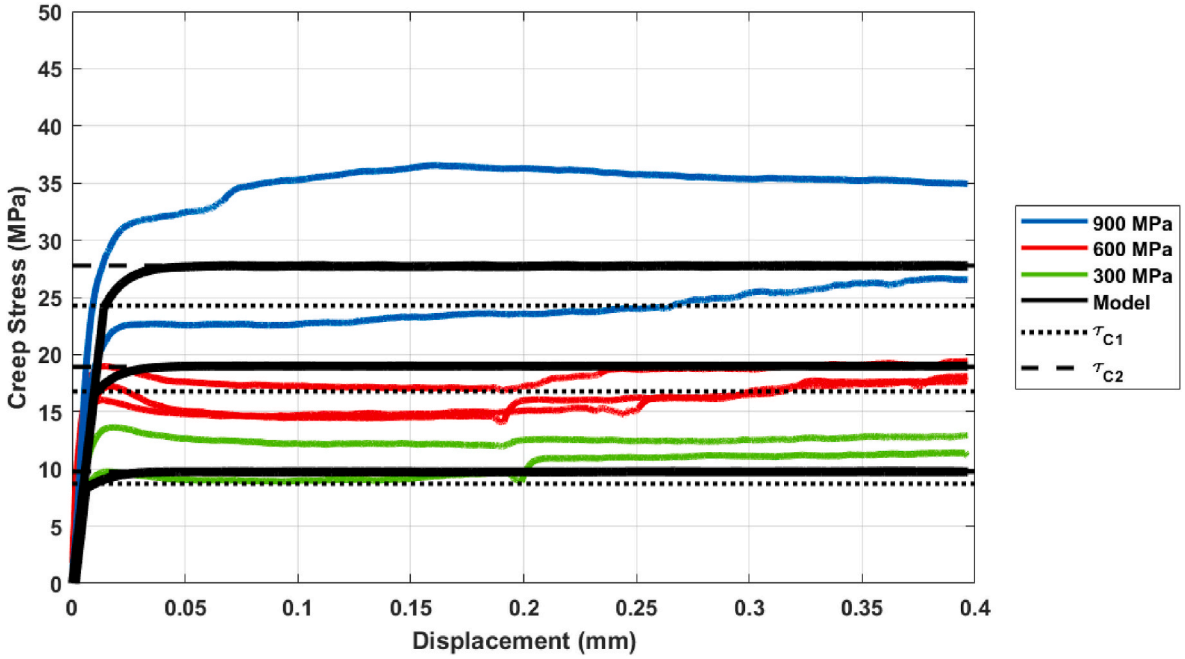


**Fig. 13.** ECF Fit for Graphite Tests with No Adhesion Material applied.

**Table 13**
ECF Input Parameters for Graphite Conditions with No Adhesion Material applied.

| Material Parameter | Nominal | Pressure Dependency |
|---|---|---|
| $L_e$ | 500 μm/GPa | $\infty\ GPa^{-1}$ |
| $L_p$ | 0.00904 mm | 209 $GPa^{-1}$ |
| $\tau_{C1}$ | 0.110 GPa | 0.275 $GPa^{-1}$ |
| $\tau_{C2}$ | 0.185 GPa | 0.181 $GPa^{-1}$ |

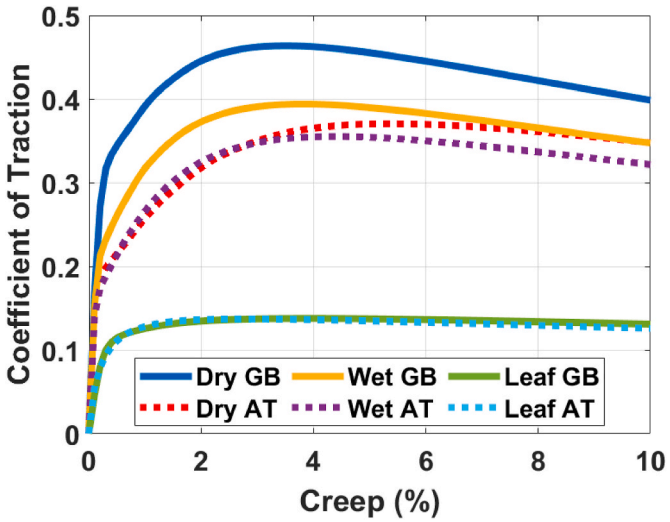


**Fig. 14.** Ecf generated creep curve predictions for British & austrian rail sands in dry, wet, and leaf contaminated conditions.

### 3.1.4. Low adhesion contaminants

The peak CoTs from HPT tests conducted with sycamore leaf and graphite are included in Table 11. Both materials produced very low adhesion, with graphite producing the slightly lower peak CoTs of the two. There appears to be very little to no pressure dependency with these low adhesion contaminants, unlike all aforementioned sanded cases.

As for sanded, leaf contaminated conditions, $L_e^0$ was parametrised again for the unsanded tests with sycamore leaf powder. The results of the fitting process are included in Fig. 12, where and relative error value of 11.8 % was calculated. Calculated shear stresses were significantly lower than all sanded tests, unsurprising as sycamore leaf is well known to act as a cause of low adhesion on the railhead [31]. As before the stiffness at lower contact pressures is over-estimated, but the critical shear stresses are fairly accurate.

The calculated input parameters for unsanded, leaf contaminated conditions are included in Table 12. As for sanded conditions, the calculated $L_e^0$ is much higher than for wet and dry conditions, again demonstrating the reduction in stiffness when a leaf layer is present in the contact.

From HPT tests conducted with the addition of graphite, the ECF model included in Fig. 13 was produced with a relative error of 20.9 %. This relatively high error value appears to come from the variation in measured shear stresses from tests conducted at 900 MPa normal pressure, however, the model still appears to fit fairly well when analysed visually. The shape and peak of the graphite curves appear different to those produced from leaf tests, with the lines in the pseudo-plastic region appearing very flat and the calculated shear stresses being generally lower. The ECF input parameters generated from the graphite, HPT tests are shown in Table 13.

### 3.2. Full-scale creep curve predictions

ECF predictions of creep curves for a full-scale wheel/rail contact generated using HPT data taken from sanded tests have been included in Fig. 14, the process for doing this was as outlined in Fig. 5. The predictions were made with the assumption of a train with a 110 kN wheel load, a 600 mm wheel diameter, and travelling at 5 m/s. The model predicted a clear difference between British and Austrian rail sands in dry conditions, with this difference becoming less pronounced in wet conditions, and practically non-existent in leaf contaminated conditions. The sanded, leaf contaminated predictions of traction compare well with previously conducted field tests [32,33].

Included in Fig. 15, are plots comparing the effect of changing wheel load on British rail sand applied in dry, wet, and leaf contaminated

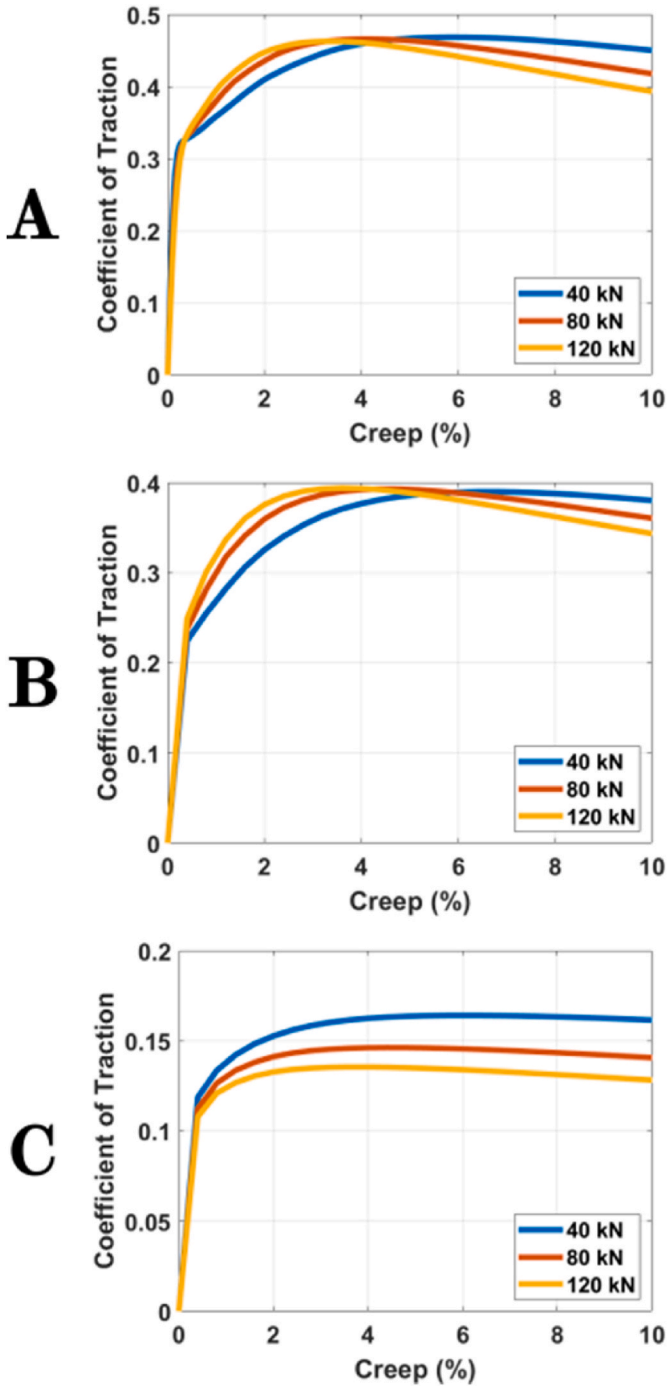


**Fig. 15.** ECF Generated Creep Curve Predictions for British Rail Sand under different Wheel Loads in: (A) Dry Conditions, (B) Wet Conditions, (C) Leaf Contaminated Conditions.

conditions respectively. In both dry and wet conditions, the peak coefficient of traction changes very little, however, the creep at which this peak occurs tends to occur at higher values for lower loads. In leaf contaminated conditions, the peak coefficient of traction increased with lower loads.

The ECF model can also be used as a means of predicting low adhesion behaviour, as demonstrated in Fig. 16, where the ECF prediction of creep curves generated from unsanded, Sycamore leaf contaminated HPT data is included. There is very little wheel load dependency exhibited, with only a very slight change in the curve shape at 40 kN. The coefficient of traction remains below 0.05 at all creep values above 2 %.

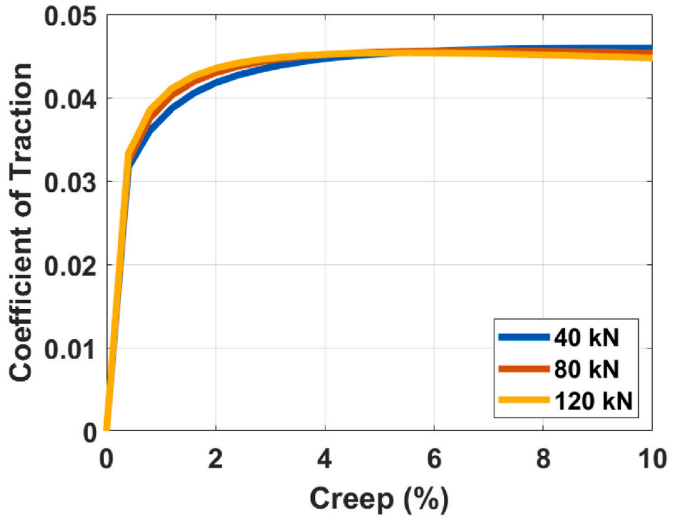


**Fig. 16.** Ecf generated creep curve predictions for sycamore leaf contaminant.

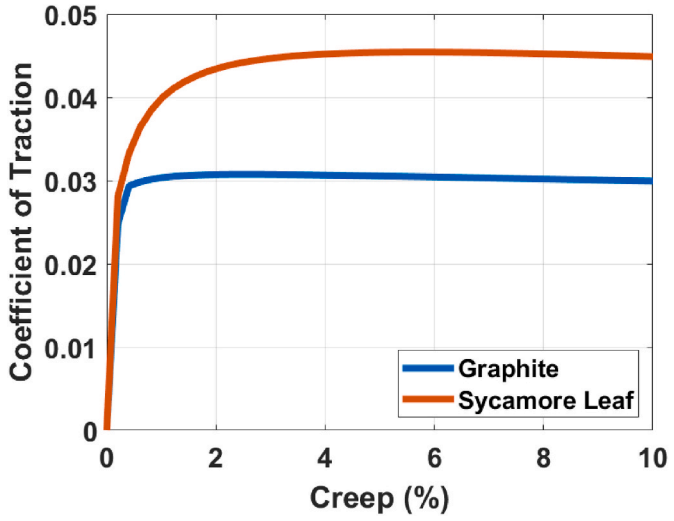


**Fig. 17.** Ecf generated creep curve predictions for graphite powder and sycamore leaf contaminant.

As a comparison of other low adhesion layers, Fig. 17 includes creep curves predicting the effect of graphite powder and sycamore leaves are included. Both materials are predicted to create low adhesion conditions, with graphite producing markedly lower traction of the two.

## 4. Discussion

### 4.1. Traction data

When sand was applied to the HPT contact, it appeared that CoTs had a pressure dependency, though the exact nature of the relationship depended on contact conditions. In both dry and wet conditions, peak CoT increased with normal pressure, whereas the opposite was true in leaf contaminated conditions.

In dry conditions, the direct relationship between increasing pressure and traction for the sanded contact was unlike that observed by Evans et al. [17], they observed that in dry, unsanded conditions, there seemed to be no clear relationship between pressure and traction. In wet conditions, the direct relationship between pressure and traction was maintained. In wet, unsanded tests conducted by Evans et al. [17], there

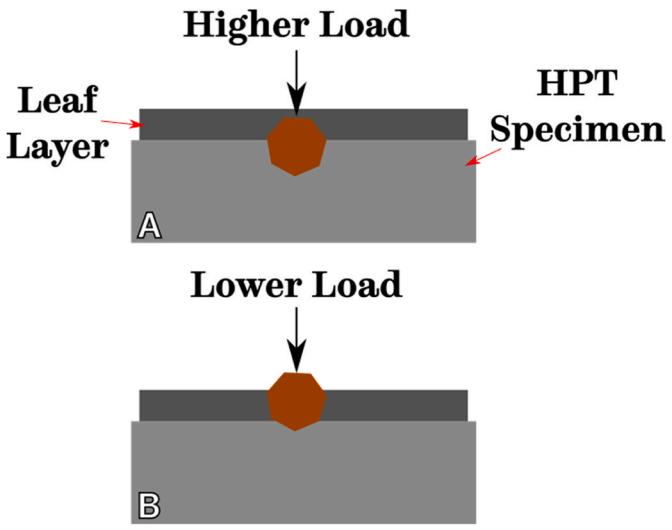


**Fig. 18.** Difference in Particle Indentation under: (a) Higher Contact Pressures; (b) Lower Contact Pressures.

**Table 14**
Summary of peak CoTs for ECF predictions and full-scale data.

| Conditions | | Peak CoT | | | |
|---|---|---|---|---|---|
| | | ECF | Meierhofer [22] | Fischer [33] | Lewis et al. [35] |
| Sanded | Dry | 0.37–0.46 | 0.3–0.4 | – | – |
| | Wet | 0.35–0.39 | 0.3–0.4 | – | – |
| | Leaf | 0.14 | – | 0.14–0.18 | – |
| Leaf | | 0.05 | – | 0.02–0.04 | 0.01–0.02 |

was no clear relationship between pressure and traction.

This trend of decreasing traction with decreasing normal pressure, apparent in both dry and wet conditions, may be due to the decreasing indentation depth of the particles as less pressure is applied and the amount of particle transferring tractive force is reduced. A similar mechanism was proposed in previous HPT testing [19] to explain the link between increasing particle hardness and increasing traction (both higher contact pressure and particle hardness would result in greater indentation depth). Similar findings relating lower normal loads, with lower friction due to less indentation were observed by Bhushan and Kulkarni [34]; they summarised that lower normal loads lead to less indentation depth, thus a lower contact area and the coefficient of friction being lower as less ploughing occurred.

In leaf contaminated conditions, as contact pressure increased the traction decreased; this was not apparent in the unsanded case. One explanation for this may be that as normal pressure increased, the particles indented further into the steel surface of the wheel and rail specimens, as posited for the dry and wet cases. However, as more the particle is indented into the wheel/rail surface there is less of the particle acting on the leaf layer itself, thus there is less material to remove the leaf layer, see Fig. 18 for a schematic representation.

### 4.2. Extended creep force model fitting accuracy

Overall the fitting of the ECF model to HPT data tended to produce error values below 15 % (with the exception of graphite data). Visually, the biggest discrepancy between fits and HPT data was at lower normal pressures and creep loads, with an overestimate of nominal inverted elastic stiffness occurring ($L_e^0$). This parameter was optimised separately from the other parameters to decrease computational expense and increase the chances of convergence to a solution, so was kept fixed during the fitting process, this may explain these errors.

The difference in nominal inverted stiffness when a leaf layer was present, unsurprisingly suggests that contact stiffness was greatly reduced when compared to the dry and wet conditions. This demonstrates how fundamentally different an HPT contact in leaf contaminated conditions behaves.

### 4.3. Full-scale validation

Traction measurement data from vehicle tests conducted with sand in dry and wet conditions were included in a thesis by Meierhofer [22], which measured a peak coefficient of traction between 0.3 and 0.4 in dry and wet sanded conditions. These measurements agree relatively well with dry and wet sanded behaviour of Austrian rail sand (see Fig. 14).

Field test results from trials conducted on leaf layers, with and without sanding [33], compare favourably with ECF generated predictions. Field trials measured a coefficient of traction 0.02–0.04 in a leaf contaminated contact, which rose to be between 0.14 and 0.18 when sand was applied; these were very similar to ECF predictions shown in Figs. 14 and 16.

The predictions of leaf behaviour also compare well with full-scale measurements where measurements of traction were recorded at 0.02 with very little variation in traction with wheel load [35]. This latter point agrees especially well with observations from Fig. 16.

A summary of the aforementioned comparisons with ECF predictions is included in Table 14. It should be noted that it was not possible to generate predictions of the exact scenarios for each set of full-scale data, due to limitations such as not knowing the exact amount of 3rd body material being applied, exact wheel profiles, condition of wheel/rail surfaces etc.

## 5. Conclusions

HPT data from two different rail sands have been used to parameterise the ECF model in dry, wet, and leaf contaminated conditions. The ECF model was then used to predict full-scale creep force – creep curves for different combinations of adhesion restoring materials and contaminants.

British rail sand was predicted to create peak adhesion levels of between, 0.4–0.5, 0.3–0.4, and 0.1–0.2 for dry, wet, and leaf contaminated conditions respectively for a typical wheel/rail contact. Austrian rail sand produced similar values with the exception of dry conditions, where the peak coefficient of traction was predicted to be between 0.3 and 0.4.

In addition, the method was used to predict creep force – creep curves for low adhesion conditions. With Sycamore leaf powder applied, a peak coefficient of traction of 0.04–0.05 was predicted and for graphite powder, this was approximately 0.03.

The ECF generated creep force – creep curves proved that differences in traction restoring performance between the rail sands could be quantified using this HPT/ECF method and predictions compared relatively well with full-scale and field data available. This approach may be useful in selecting and assessing adhesion restoring materials before validating with field testing, as well as the predicted full-scale creep force – creep curves being useful for integration into multi-body dynamics simulations to assess train performance, braking, etc.

Future work would focus on parameterising the ECF model with more types of adhesion restoring material and/or low adhesion contaminants. In addition, more full-scale would be required for validation.

## CRediT authorship contribution statement

**W. Skipper:** Writing – review & editing, Writing – original draft, Visualization, Validation, Methodology, Investigation, Formal analysis. **A. Meierhofer:** Writing – review & editing, Visualization, Validation, Methodology, Formal analysis. **A. Chalisey:** Writing – review & editing, Supervision, Resources. **K. Six:** Writing – review & editing, Supervision,

Conceptualization. **R. Lewis:** Writing – review & editing, Supervision, Project administration, Conceptualization.

## Declaration of competing interest

The authors certify that they have NO affiliations with or involvement in any organization or entity with any financial interest (such as honoraria; educational grants; participation in speakers' bureaus; membership, employment, consultancies, stock ownership, or other equity interest; and expert testimony or patent-licensing arrangements), or non-financial interest (such as personal or professional relationships, affiliations, knowledge or beliefs) in the subject matter or materials discussed in this manuscript.

## Data availability

Data will be made available on request.

## Acknowledgements

This work was supported by the Engineering and Physical Sciences Research Council (UK) and Rail Safety Standards Board (UK) (grant number EP/L01629X/1). In addition, part of this work was sponsored by the EPSRC knowledge exchange scholarship. The publication was written with the support of Virtual Vehicle Research GmbH in Graz, Austria. The authors would like to acknowledge the financial support within the COMET K2 Competence Centres for Excellent Technologies from the Austrian Federal Ministry for Climate Action (BMK), the Austrian Federal Ministry for Digital and Economic Affairs (BMDW), the Province of Styria and the Styrian Business Promotion Agency (SFG). The Austrian Research Promotion Agency (FFG) has been authorised for the programme management. The authors would also like to thank The Rail Safety and Standards Board for their guidance throughout the project. For the purpose of open access, the author has applied a Creative Commons Attribution (CC BY) license to any Author Accepted Manuscript version arising.

## References

[1] C.R. Fulford, Review of Low Adhesion Research (T354), RSSB Report), 2004.
[2] Rail Accident Investigation Branch, Autumn Adhesion Investigation Part 3: Review of Adhesion-Related Incidents Autumn 2005, RAIB Report), 2007.
[3] P. Gray, T1107 Sander Trials Dissemination Event, 2018 [Online]. Available: https://www.rssb.co.uk/Pages/adhesion.aspx.
[4] W.A. Skipper, A. Chalisey, R. Lewis, A review of railway sanding system research: adhesion restoration and leaf layer removal, Tribol. Mater. Surface Interfac. 12 (4) (2018) 237–251.
[5] O. Arias-Cuevas, Z. Li, R. Lewis, E.A. Gallardo-Hernández, Laboratory investigation of some sanding parameters to improve the adhesion in leaf-contaminated wheel–rail contacts, J. Rail Rapid Transit 224 (3) (2010) 139–157.
[6] Z. Li, O. Arias-Cuevas, R. Lewis, E.A. Gallardo-Hernández, Rolling–Sliding laboratory tests of friction modifiers in leaf contaminated wheel–rail contacts, Tribol. Lett. 33 (2) (2009) 97–109.
[7] O. Arias-Cuevas, Z. Li, R. Lewis, E.A. Gallardo-Hernández, Rolling–sliding laboratory tests of friction modifiers in dry and wet wheel–rail contacts, Wear 268 (3–4) (2009) 543–551.
[8] O. Arias-Cuevas, Z. Li, R. Lewis, A laboratory investigation on the influence of the particle size and slip during sanding on the adhesion and wear in the wheel-rail contact, Wear 271 (1–2) (2010) 14–24.
[9] E.A. Gallardo-Hernandez, R. Lewis, Twin disc assessment of wheel/rail adhesion, Wear 265 (9–10) (2008) 1309–1316.
[10] R. Lewis, R.S. Dwyer-Joyce, Wear at the wheel/rail interface when sanding is used to increase adhesion, J. Rail Rapid Transit 220 (1) (2006) 29–41.
[11] R. Lewis, R.S. Dwyer-Joyce, J. Lewis, Disc machine study of contact isolation during railway track sanding, J. Rail Rapid Transit 217 (1) (2003) 11–24.
[12] A. Meierhofer, C. Hardwick, R. Lewis, K. Six, P. Dietmaier, Third body layer-experimental results and a model describing its influence on the traction coefficient, Wear 314 (1–2) (2014) 148–154.
[13] K. Edalati, Z. Horita, A review on high-pressure torsion (HPT) from 1935 to 1988, Mater. Sci. Eng., A 652 (2015) 325–352.
[14] A. Hohenwarter, R. Pippan, Sample size and strain-rate-sensitivity effects on the homogeneity of high-pressure torsion deformed disks, Metall. Mater. Trans. A Phys. Metall. Mater. Sci. 50 (2) (2019) 601–608.
[15] T. Leitner, G. Trummer, R. Pippan, A. Hohenwarter, Influence of severe plastic deformation and specimen orientation on the fatigue crack propagation behavior of a pearlitic steel, Mater. Sci. Eng., A 710 (2018) 260–270. October 2017.
[16] R. Pippan, S. Scheriau, A. Hohenwarter, M. Hafok, Advantages and limitations of HPT: a review, Mater. Sci. Forum 584–586 (2008) 16–21. January.
[17] M. Evans, W.A. Skipper, L. Buckley-Johnstone, A. Meierhofer, K. Six, R. Lewis, The development of a high pressure torsion test methodology for simulating wheel/rail contacts, Tribol. Int. 156 (Apr. 2021) 106842, 106842.
[18] W.A. Skipper, S. Nadimi, A. Chalisey, R. Lewis, Particle characterisation of rail sands for understanding tribological behaviour, Wear 432–433 (2019) 202960.
[19] W.A. Skipper, S. Nadimi, M. Watson, A. Chalisey, R. Lewis, Quantifying the effect of particle characteristics on wheel/rail adhesion & damage through high pressure torsion testing, Tribol. Int. 179 (2022) 108190.
[20] W. Skipper, et al., Investigating the effect of different adhesion materials on electrical resistance using a high pressure torsion rig, in: 12th International Conference on Contact Mechanics and Wear of Rail/wheel Systems, 2022, pp. 528–534.
[21] D. Kvarda, R. Galas, M. Omasta, M. Hartl, I. Krupka, M. Dzimko, Shear properties of top-of-rail products in numerical modelling, Proc. Inst. Mech. Eng. - Part F J. Rail Rapid Transit 0 (0) (Nov. 2022) 1–10.
[22] A. Meierhofer, A New Wheel-Rail Creep Force Model Based on Elasto-Plastic Third Body Layers (PhD Thesis), TU Graz, 2015.
[23] M.D. Evans, Performance Assessment of Friction Management Products in the Wheel-Rail Interface (PhD Thesis), University of Sheffield, 2018.
[24] Adhesion Working Group, Managing Low Adhesion, 2018 [Online]. Available: https://www.raildeliverygroup.com/media-centre-docman/121-2018-01-managing-low-adhesion-ed6-0/file.html. (Accessed 22 November 2021).
[25] Rail Safety and Standards Board, GMRT2461 Sanding Equipment (Issue 3), https://www.rssb.co.uk/standards-catalogue/CatalogueItem/gmrt2461-iss-3-1, 2018.
[26] S. Maramizonouz, S. Nadimi, W. Skipper, R. Lewis, Characterisation of physical and mechanical properties of seven particulate materials proposed as traction enhancers, Sci. Data 10 (1) (Jun. 2023) 400.
[27] K. Ishizaka, B. White, M. Watson, S.R. Lewis, R. Lewis, Influence of temperature on adhesion coefficient and bonding strength of leaf films: a twin disc study, Wear 454–455 (Aug. 2020) 203330.
[28] K. Six, et al., Plasticity in wheel-rail contact and its implications on vehicle-track interaction, Proc. Inst. Mech. Eng. - Part F J. Rail Rapid Transit 231 (5) (2017) 558–569.
[29] I. Goryacheva, F. Sadeghi, Contact characteristics of a rolling/sliding cylinder and a viscoelastic layer bonded to an elastic substrate, Wear 184 (2) (May 1995) 125–132.
[30] S. Alexandrov, A property of equations of rigid/plastic material obeying a voce-type hardening law, Meccanica 34 (1999) 349–356.
[31] K. Ishizaka, S.R. Lewis, R. Lewis, The low adhesion problem due to leaf contamination in the wheel/rail contact: bonding and low adhesion mechanisms, Wear 378 (379) (2017) 183–197.
[32] L. Purcell, A. Lightoller, Trial of Sander configurations and sand laying rates (T1107) (RSSB report) [Online]. Available: https://www.rssb.co.uk/research-catalogue/CatalogueItem/IMP-T1107, 2018.
[33] M. Fischer, K. Haselsteiner, F. Szekely, S. Heinz, F. Kröger, Mehr Mobilität auf der Schiene: Erhöhung der Transportkapazität durch Optimierung des Kraftschlusses, ZEVrail, 2020.
[34] B. Bhushan, A.V. Kulkarni, Effect of normal load on microscale friction measurements, Thin Solid Films 278 (1–2) (May 1996) 49–56.
[35] R. Lewis et al., "Leaves on the Line: Characterising Leaf Based Low Adhesion on Railway Rails," Submitt. Publ..